I&EC research
Industrial & Engineering Chemistry Research

Article

pubs.acs.org/IECR

Assessment of Integral Thermo-Hydraulic Models for Pipeline Transportation of Dense-Phase and Supercritical CO_2

Sergey Martynov,*[,†] Niall Mac Dowell,[‡,§] Solomon Brown,[†] and Haroun Mahgerefteh*[,†]

[†]Department of Chemical Engineering, University College London, Torrington Place, London WC1E 7JE, United Kingdom
[‡]Centre for Environmental Policy, Imperial College London, London SW7 1NA, United Kingdom
[§]Centre for Process Systems Engineering, Imperial College London, London SW7 2AZ, United Kingdom

ABSTRACT: The accurate design and economic evaluation of a high-pressure CO_2 pipeline transportation network employed as part of any Carbon Capture and Sequestration (CCS) chain requires the availability of reliable thermo-hydraulic models for predicting the pressure drop and temperature and ultimately the fluid phase in a pipeline. In this study, the performance of a number of integral thermo-hydraulic models is examined on the basis of the comparison of their predictions against those obtained using a validated, more rigorous but computationally demanding numerical one-dimensional steady-state flow model. The study is performed for typical 0.4−1.2 m internal diameter pipelines transporting CO_2 over distances of up to 100 km at supercritical pressures ranging from 90 to 170 bar and temperatures from 20 to 60 °C. Buried, insulated, and noninsulated above-ground horizontal pipelines are considered in the analysis. The study concludes that, of the integral models examined, (1) the model based on the nonisothermal compressible flow equation for the pressure drop, combined with the temperature equation accounting for the Joule−Thomson effect and heat exchange at the pipe wall, provides the most accurate model; (2) the model which uses the Darcy−Weisbach equation and accounts for the density variation with the temperature and pressure in the pipe provides a simple method with comparable performance with the first method; (3) using the Darcy−Weisbach equation with constant density can lead to very large errors in pressure drop calculations.

1. INTRODUCTION

Carbon Capture and Sequestration (CCS) has been proposed as a promising technology for the mitigation of CO_2 emissions into the atmosphere from fossil-fuel-operated power generation plants.[1−3] Importantly, each of the individual links in the CCS chain are technically mature, and there are several commercial-scale CCS projects currently planned or in operation around the world.[4−7] In such projects, to enable large-scale and long-distance transportation of the captured CO_2 from different point-source emitters to locations for secure geological sequestration, high-pressure pipeline networks are considered the most economically viable option.[8,9]

The cost associated with the design and operation of CCS systems has received considerable attention.[1,10−12] Although estimates vary, it is generally accepted that the capture cost dominates the total cost, followed by compression and then storage.[13−15] Ironically, despite its importance, relatively little attention has been paid to the development of cost estimation tools for CO_2 transport pipeline networks, with CO_2 transport often being accorded a fixed cost per unit mass transported per unit distance.[16]

Most of the existing cost models are built on conservative pipeline design assumptions, using simple correlations relating the pipeline diameter with the flow rate and frictional pressure drop, largely neglecting realistic conditions for CO_2 pipeline transportation in the CCS chain.[9,17−22] In particular, a modification in the design or operation of the capture process may affect the pressure or composition of the CO_2 stream and consequently the outlet pressure of the compressor as well as the inlet pressure to the pipeline transport system. Similarly, seasonal variations in the ambient temperature and humidity will affect the heat exchange with the pipe wall and subsequently the possibility of a thermo-hydraulically induced phase transition.[23] In the case of CO_2 pipeline transportation, a number of recent studies[24−27] have indicated the subsequent significant impact of a phase change on the pressure drop and, hence, the compression costs. As the reliability and cost effectiveness of the pipeline transport network is pivotal to the overall operability and resilience of the CCS system, it is vital that the models employed for the design and evaluation of these networks accurately describe the thermo-hydraulic behavior of these systems for a wide range of operating conditions.

Simple and robust algebraic pressure drop correlations are required for the engineering pipeline design and optimization modeling, where using more rigorous pipeline flow models based on the differential form of conservation equations[28,29] is more computationally demanding and, hence, is less practical.[26,30] These algebraic models provide an "integral" representation of the conservation equations, which are commonly expressed using the Bernoulli equation and frictional pressure drop models for isothermal flow (e.g., Panhandle, Weymouth, and AGA equations[31,32]), widely used in the design of pipelines transporting natural gas and incompressible liquids. However, the properties of CO_2 fluid at supercritical pressures (i.e., at pressures above 73.9 bar) and temperatures in the range from 0 to 60 °C relevant for the pipeline transportation differ

Received: March 4, 2015
Revised: August 4, 2015
Accepted: August 7, 2015
Published: August 7, 2015

DOI: 10.1021/acs.iecr.5b00851
Ind. Eng. Chem. Res. 2015, 54, 8587−8599

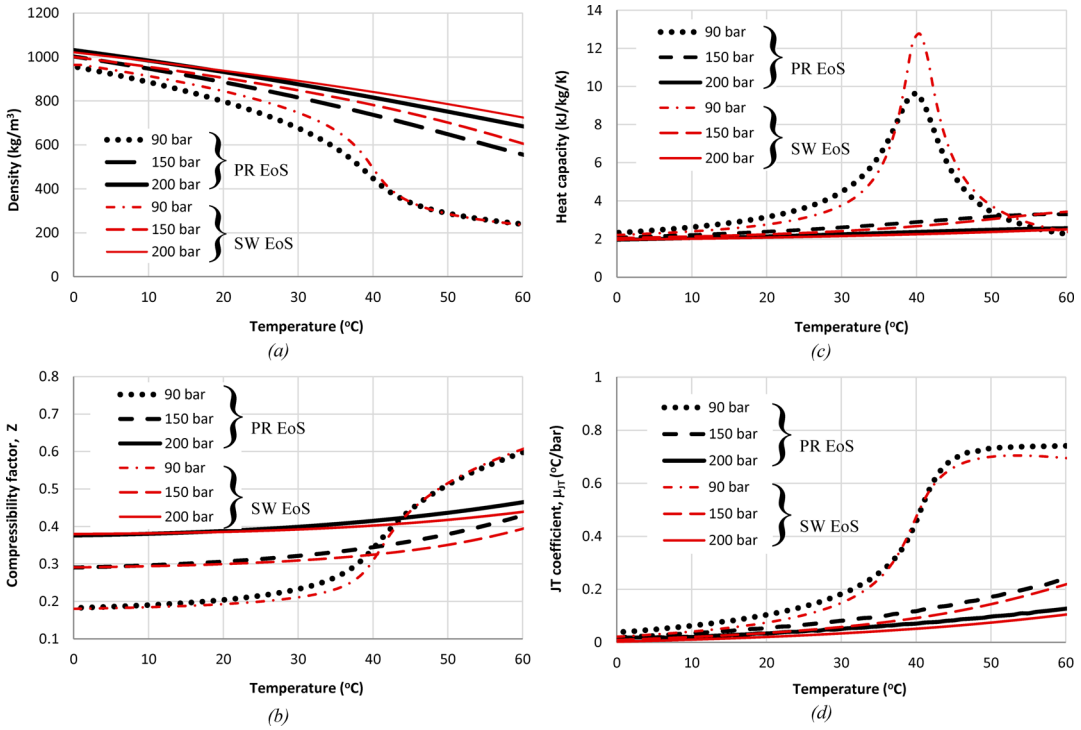

Figure 1. Variation of the density (a), compressibility (b), heat capacity (c), and Joule−Thomson coefficient (d) of pure CO_2 with temperature at pressures of 90, 150 to 200 bar. Predictions using the PR EoS and SW EoS in REFPROP.[37]

significantly from those for a hydrocarbon gas or an incompressible liquid. In turn, strong variation of the physical properties of CO_2 with pressure and temperature along the pipe may invalidate the assumptions of the pressure drop correlations, reducing the accuracy of their predictions.[19,21,33] As such, systematic validation of integral thermo-hydraulic models is of significant practical interest for the CO_2 pipeline networks design in CCS.[34]

The main objective of this study is to examine existing integral thermo-hydraulic models for the calculation of pressure drop and temperature variation in pipelines transporting dense-phase and supercritical CO_2 for CCS. Although transported CO_2 may contain some amounts of impurities, for the purpose of the present study, it is assumed that the fluid is pure CO_2. To validate the integral models, the results of their application are compared with predictions using a rigorous one-dimensional steady-state model for flow in a pipeline.

The paper is organized as follows. Section 2 gives a brief account of the thermodynamic properties of supercritical and dense-phase CO_2, relevant to the thermo-hydraulic analysis of pipeline transportation. Section 3 describes the rigorous one-dimensional steady-state flow (ODSF) model for benchmarking the integral thermo-hydraulic models presented in Section 4. Section 5 describes the methodology of the study, while Section 6 presents the results of the evaluation of the effects of inlet pressure and temperature, heat transfer, and pipe length on the performance of the various integral thermo-hydraulic models for calculation of flow in high-pressure pipelines transporting CO_2 fluid. Conclusions for the study and discussion of the practical implications of the results are presented in Section 7.

2. PHYSICAL PROPERTIES OF CO_2

The most economically efficient mode for pipeline transportation of CO_2 is in its liquid or dense-phase supercritical states.[9,24] To reach these conditions, the minimum pipeline operating pressure is commonly set to at least 10 bar above the fluid critical pressure. For almost pure CO_2, which has critical pressure of 73.4 bar, the recommended minimum operating pressure is 86 bar.[9] The maximum pipeline operation pressure for onshore pipelines is commonly set below 150 bar,[35] whereas for offshore pipelines, this pressure can be as high as 300 bar.[16] The pipeline operating temperatures are affected by both the temperature of the CO_2 stream after the primary compressor and the temperature of the medium surrounding the pipeline (i.e., air, water, or soil). The latter is a function of a number of variables, including the type of soil through which the pipeline is traveling, the water saturation of that soil and the time of year. In the case of an off-shore pipeline this depends on the depth below the sea level. Although in the European climate, a temperature range of 0 to 20 °C seems likely,[9,36] in warmer regions, the ground surface temperature in direct sunlight can reach 65 °C.[24] The range of CO_2 pipeline inlet temperatures is usually confined to 0−60 °C.[24]

The key thermo-physical properties determining the pressure drop and temperature variation in pipelines transporting gases and liquids are density, compressibility, heat capacity, and Joule−Thomson coefficient. Although in the case of liquid transportation pipes the fluid compressibility and Joule−Thomson effects are generally neglected in the thermo-hydraulic models, they are all important for simulation of flows in gas transmission pipes. Importantly, in the case of supercritical fluids, their properties differ significantly from those of gases and liquids. In the case of pure CO_2, its thermodynamic properties in liquid, vapor, and supercritical states may be reasonably accurately predicted using cubic

DOI: 10.1021/acs.iecr.5b00851
Ind. Eng. Chem. Res. 2015, 54, 8587−8599

equations of state. In this study, the translated Peng−Robinson equation of state (PR EoS), as implemented in REFPROP package,[37] is employed given its proven accuracy in modeling vapor−liquid behavior of CO_2,[38,39] relative simplicity, and computational efficiency.

Figure 1 shows the physical properties for CO_2 predicted for the range of pressures and temperatures relevant to the CO_2 pipeline transportation using the PR EoS in comparison with the properties based on the Span and Wagner (SW) EoS,[40] which provides the most accurate empirical fit of the data for pure CO_2. These properties include the density, ρ, heat capacity, c_p, as well as the compressibility factor, Z, and the Joule−Thomson coefficient, μ_{JT}, which are defined as

$$Z \underline{\underline{\text{def}}} \frac{p}{\rho R T} \tag{1}$$

$$\mu_{JT} \underline{\underline{\text{def}}} \left(\frac{\partial T}{\partial p}\right)_h = \frac{R T^2}{p c_p}\left(\frac{\partial Z}{\partial T}\right)_p \tag{2}$$

where p, T, h and R are, respectively, the fluid pressure, temperature, enthalpy, and the gas constant of CO_2.

As can be seen in Figure 1, for the range of pressures and temperatures studied, the PR EoS captures the behavior of the various physical properties of CO_2 with temperature and pressure in a good agreement with the SW EoS data. As it may be further observed from Figure 1, at 90 bar, the variation of the thermo-physical properties of CO_2 with temperature becomes highly nonlinear. In particular, in accordance with Figure 1c, as the temperature approaches ca. 20 °C, the heat capacity increases dramatically, reaching a peak value at ca. 40 °C, followed by a rapid drop at higher temperatures. This is accompanied by a significant increase in the Joule-Thomson coefficient (by more than 300%: Figure 1d), the fluid compressibility (ca. 50% increase: Figure 1b) and decrease in density (ca. 50% drop: Figure 1a). Remarkably, as the temperature falls below ca. 40 °C, the fluid compressibility (Figure 1b) increases with pressure, while at any temperature above ca. 40 °C the compressibility goes through a minimum when the pressure changes from 90 to 200 bar.

In Figure 1, the properties of CO_2 fluid at supercritical pressures vary from those typical for gas to those of the liquid phase. The transition from liquid-like to gas-like properties strongly depends on the pressure and temperature and may be accompanied by a peak in the heat capacity and significant changes in density with the temperature. As such, the application of existing thermo-hydraulic models, developed either for gas or liquid pipelines, to supercritical CO_2 requires careful assessment of the underlying assumptions of such models to ensure that the above behavior of the properties is adequately taken into account.

3. ONE-DIMENSIONAL STEADY-STATE FLOW (ODSF) MODEL

Transportation of a compressible fluid such as supercritical or dense-phase CO_2 in a long pipeline may result in significant changes in its pressure and temperature due to the effects of frictional pressure drop, expansion work by the fluid, and heat exchange with the surroundings. To simulate the flow and heat transfer of single-phase fluid at supercritical pressures in horizontal pipes taking account of the above effects, a one-dimensional flow model, governed by the following respective mass, momentum, and energy conservation equations is employed:[41]

$$\frac{\mathrm{d}\rho u}{\mathrm{d}x} = 0 \tag{3}$$

$$\frac{\mathrm{d}\rho u^2}{\mathrm{d}x} = -\frac{\mathrm{d}p}{\mathrm{d}x} - f\frac{\rho u^2}{2D} \tag{4}$$

$$\frac{\mathrm{d}\rho u\left(h + \frac{1}{2}u^2\right)}{\mathrm{d}x} = \frac{4q_w}{D} + f\frac{\rho u^3}{2D} \tag{5}$$

where x and D are, respectively, the local coordinate along the pipeline and the pipeline inner diameter, while u, f, and q_w are is the local velocity of the flow, the Darcy friction factor, and the heat flux at the pipe wall.

In eq 4, the first term on the right-hand side is the local pressure gradient. This pressure gradient is balanced by the inertial term on the left-hand side and the second term on the right-hand side, describing the effect of viscous friction at the pipe wall.

Equation 5 describes the change in the flux of total enthalpy, $h + (1/2)u^2$, along the pipe due to the heat exchange at the pipe wall, as described by the first term on the right-hand side, and the viscous dissipation in the flow, as accounted by the second term on the right-hand side.

For turbulent flow in a straight pipe, the friction factor, f, can be calculated using the modified Colebrook−White equation:[42]

$$f = 0.25\left[\lg\left(\frac{\epsilon}{3.7D} + \frac{5.74}{\mathrm{Re}^{0.9}}\right)\right]^{-2} \tag{6}$$

where, ϵ and $\mathrm{Re} = \overline{\rho u}\, D/\mu_f$ are the wall roughness and the flow Reynolds number, respectively, while $\overline{\rho u}$ and μ_f are the average mass flux and the coefficient of the dynamic viscosity of the fluid.

The heat flux at the pipe wall, q_w, is defined via the heat transfer equation:

$$q_w = \alpha(T_f - T_a) \tag{7}$$

where T_a and T_f are, respectively, the temperatures of the media surrounding the pipe and the fluid inside the pipe, and α is the overall heat transfer coefficient. In the general case of a buried pipeline, the overall heat transfer coefficient is defined as[43]

$$\alpha = \left[\frac{1}{\alpha_f} + \frac{D}{2\lambda_w}\ln\left(\frac{D_o}{D}\right) + \frac{D}{2\lambda_s}\ln\left(\frac{z_s}{D}\right) + \frac{1}{\alpha_a}\frac{D}{2z_s}\right]^{-1} \tag{8}$$

where D_o is the external diameter of the pipe, λ_w and λ_s are the thermal conductivities of the pipe wall and the soil respectively; z_s is the depth at which the pipeline is buried, measured from the pipeline axis to the surface of the ground, while α_f and α_a are respectively the heat transfer coefficients on both the internal and external sides of the pipe wall. In the present study, α_a is assumed to be constant, while α_f is calculated using the Dittus−Boelter correlation for turbulent forced convection in pipes:[43]

$$\alpha_f = 0.023\mathrm{Re}^{0.8}\mathrm{Pr}^{0.4}\frac{\lambda_f}{D} \tag{9}$$

where $\mathrm{Pr}_f = \mu c_p/\lambda_f$ is the fluid Prandtl number and λ_f is the thermal conductivity of the fluid.

DOI: 10.1021/acs.iecr.5b00851
Ind. Eng. Chem. Res. 2015, 54, 8587−8599

Equations 3−9 together with the relations required to calculate the relevant thermophysical properties and specified flow conditions (e.g., the mass flow rate $\overline{\rho u}$ and the fluid inlet temperature, T_{in}, and pressure, p_{in}) form a set of differential-algebraic equations, which are solved numerically to obtain the fluid pressure, temperature, and velocity profiles along the pipeline. For this purpose, in the present study, a FORTRAN code is built using the DASSL differential and algebraic equations solver.[44]

Despite the fact that the one-dimensional models account for the important processes governing the fluid flow within the pipeline, their solution requires application of suitable numerical methods thus making them computationally demanding. For this reason, the one-dimensional models are not routinely employed in the pipeline design practice, where simpler integral thermo-hydraulic models are used instead.[9,17,18,32,45−47]

4. INTEGRAL THERMO-HYDRAULIC MODELS

The following presents an overview of commonly employed integral thermo-hydraulic models for the determination of the fluid pressure drop and the temperature change along the pipeline. These models result from integration of the differential momentum and energy balance eqs 4 and 5 incorporating various assumptions as detailed next.

4.1. Pressure Drop Models. *Model 1: Nonisothermal Compressible Flow.* To calculate the pressure drop in a pipeline transporting compressible fluid, the following form of integral momentum equation is commonly applied in the case of nonisothermal flow:[48]

$$\frac{p_{in}^2 - p_{out}^2}{2(\overline{\rho u})^2} = \overline{\left(\frac{p}{\rho}\right)}\frac{\overline{f}}{2}\frac{L}{D} + \overline{\left(\frac{p}{\rho}\right)}\ln\left(\frac{p_{in}}{p_{out}}\right) - \left(\frac{p_{in}}{\rho_{in}} - \frac{p_{out}}{\rho_{out}}\right) \tag{10}$$

which can also be written as

$$p_{in} - p_{out} = \underbrace{\left(\frac{(\overline{\rho u})^2}{\overline{p}}\right)\overline{\left(\frac{p}{\rho}\right)}\frac{\overline{f}}{2}\frac{L}{D}}_{\Delta p_{fr}} + \underbrace{\left(\frac{(\overline{\rho u})^2}{\overline{p}}\right)\overline{\left(\frac{p}{\rho}\right)}\ln\left(\frac{p_{in}}{p_{out}}\right)}_{\Delta p_c} - \underbrace{\left(\frac{(\overline{\rho u})^2}{\overline{p}}\right)\left(\frac{p_{in}}{\rho_{in}} - \frac{p_{out}}{\rho_{out}}\right)}_{\Delta p_\rho} \tag{11}$$

where $\overline{\left(\frac{p}{\rho}\right)}$ and $\overline{f}$ are, respectively, the pressure to density ratio and friction factor averaged along the pipeline length L. The first term on the right-hand side of eq 10, Δp_{fr}, represents the frictional pressure drop, the second term, Δp_c, describes the effect of the fluid compressibility, whereas the third term, Δp_ρ, accounts for the effect of compressibility and the density variation along the pipe. Commonly, $\overline{f}$ is calculated using the local friction factor correlations, where the fluid properties are taken at the average pressure and temperature for the flow, which are usually defined as the algebraic average of the inlet and outlet values:[32,35]

$$\overline{p} = \frac{p_{in} + p_{out}}{2} \tag{12}$$

$$\overline{T} = \frac{T_{in} + T_{out}}{2} \tag{13}$$

Similarly, the ratio $\overline{\left(\frac{p}{\rho}\right)}$ in eqs 10 and 11 is defined as

$$\overline{\left(\frac{p}{\rho}\right)} = \frac{1}{2}\left(\frac{p_{in}}{\rho_{in}} + \frac{p_{out}}{\rho_{out}}\right)$$

As the compressible flow expands and accelerates along the pipe, the flow can become choked.[49] This phenomenon is accompanied by significant local pressure gradients which can be resolved by the ODSF model, but it cannot be captured accurately by integral pressure drop models. As such, an additional criterion is needed to ensure validity of the integral pressure drop models. This can be based either on a conventional Mach number criterion ($M = u/c_s$), which requires $M < 1$ for subsonic flow in the pipe, or ensuring that the pipeline length is smaller than the "critical" pipe length, L_{ch}, for which the flow is choked: $L < L_{ch}$. Although there are no expressions for L_{ch} for the general case of compressible flow in a pipe, it can be estimated using the closed-form solution for an adiabatic flow of ideal gas (Fanno flow):[49]

$$L_{ch} = \frac{D}{4\overline{f}\,\gamma}\left[\frac{1 - M^2}{M^2} + \frac{1 + \gamma}{2}\ln\frac{(\gamma + 1)M^2}{2 + (\gamma - 1)M^2}\right] \tag{14}$$

where γ is the adiabatic index of the gas and $M = u_{in}/c_s$ is Mach number based on the inlet velocity, and c_s is the speed of sound.

Model 2: Isothermal Compressible Flow. In case of isothermal flow of gases, using equation of state expression $p/\rho = ZRT$ and also assuming that the fluid compressibility, Z, does not change significantly with pressure, eq 10 may be written as[32]

$$\frac{p_{in}^2 - p_{out}^2}{2\overline{\rho u}^2} = \overline{Z}RT\left[\frac{\overline{f}}{2}\frac{L}{D} + \ln\left(\frac{p_{in}}{p_{out}}\right)\right] \tag{15}$$

where $\overline{Z}$ is the average compressibility which is as a function of the average $\overline{p}$ (see below) and T. In order to account for nonlinear variation of the gas compressibility $\overline{Z}$ with pressure, the following equation is often used to evaluate the average pressure along the pipeline:[32]

$$\overline{p} = \frac{2}{3}\frac{p_{in}^3 - p_{out}^3}{p_{in}^2 - p_{out}^2} \tag{16}$$

The difference between the average pressures defined by eqs 12 and 16 becomes significant only for flows characterized by very large pressure ratios (p_{in}/p_{out}). In the case of CO_2 pipeline transmission, the pipeline pressures are expected to vary in the range from 200 bar at the pipe inlet to 80 bar at the delivery point, corresponding to $p_{in}/p_{out} = 2.5$, for which predictions by eqs 12 and 16 deviate by less than 4.3%. Hence, eq 12 can be applied without significant impact on the accuracy of pressure drop calculations.

It is to be noted that an alternative version of eq 15, where the second term on the right-hand side is omitted and an additional term is added to account for the hydrostatic pressure head, forms the basis for the calculation of the required diameter in gas-phase transportation pipelines.[9,35]

Model 3: Isothermal Incompressible Flow. In case of incompressible liquids, the second and third terms in eq 10

DOI: 10.1021/acs.iecr.5b00851
Ind. Eng. Chem. Res. 2015, 54, 8587−8599

vanish, leading to the Darcy–Weisbach equation for the pipeline frictional pressure drop:[32]

$$p_{in} - p_{out} = \overline{f}\,\frac{\overline{\rho u}^2}{2\overline{\rho}}\,\frac{L}{D} \tag{17}$$

The above equation can also be applied to incompressible flows of gases when the pressure drop is less than 5–10% of the upstream pressure.[32] In this case, however, the density variation with temperature and pressure needs to be taken into account, e.g. by evaluating the density $\overline{\rho}$ at the average pressure and temperature as defined by eqs 12 and 13.[32]

Equation 17 is commonly applied to relate the pipeline diameter with the pressure drop in the pipeline design models.[45−47]

4.2. Temperature Variation Models. *Model A: Flow with Heat Transfer and Expansion Cooling.* At substantially subsonic flow velocities, typical for the pipeline transportation (1.5–4 m/s for liquid-phase and 15–40 m/s for gas-phase transportation[32]), the viscous dissipation term on the right-hand side of the energy eq 5 may be assumed to be negligible. In this case eq 5 reduces to

$$\overline{\rho u}\frac{dh}{dx} = \frac{4q_w}{D} \tag{18}$$

Integrating the above equation along the pipeline gives

$$h_{out} - h_{in} = \frac{4\overline{q}_w}{\overline{\rho u}}\,\frac{L}{D} \tag{19}$$

where the average heat flux, $\overline{q}_w$, is defined using the average values of the heat transfer coefficient, $\overline{\alpha}$, the fluid temperature, $\overline{T}$, and the ambient temperature, $\overline{T}_a$:

$$\overline{q}_w = \overline{\alpha}(\overline{T}_a - \overline{T}) \tag{20}$$

Equations 10 and 19 are nonlinear algebraic equations which can be solved numerically together with the thermodynamic relations for the fluid enthalpy $h(p, T)$ and density $\rho(p, T)$ to obtain the fluid pressure and temperature at the pipeline outlet.

To obtain an explicit equation for temperature variation in the pipeline, it is useful to express eq 18 in terms of temperature using the thermodynamic relation:

$$dh = c_p(dT - \mu_{JT}dp) \tag{21}$$

Substituting this relationship into eq 18 gives

$$dT = \mu_{JT}dp + \frac{4q_w}{\overline{\rho u}c_p D}dx \tag{22}$$

Integration of this equation along the pipe length gives

$$T_{in} - T_{out} = \underbrace{\overline{\mu_{JT}}(p_{in} - p_{out})}_{\Delta T_{JT}} + \underbrace{\frac{-4q_w}{\overline{\rho u}\,\overline{c}_p}\,\frac{L}{D}}_{\Delta T_{qw}} \tag{23}$$

where $\overline{\mu_{JT}}$ and $\overline{c}_p$ are the Joule–Thomson coefficient and heat capacity of the fluid averaged along the pipe. On the right-hand side of this equation the first term, ΔT_{JT}, defines the temperature change due to the Joule–Thomson effect, while the second term, ΔT_{q_w}, is associated with convective heat exchange between the flowing fluid and the surrounding through the pipe wall.

Model B: Flow with Heat Transfer. In cases when the fluid Joule–Thomson effect can be neglected (e.g., when the fluid behaves as an ideal gas or incompressible liquid), substituting eq 20 into eq 22 with subsequent integration along the pipe length gives[31]

$$T_{out} = \overline{T}_a + (T_{in} - \overline{T}_a)\exp\left(-\frac{4\overline{\alpha}}{\overline{\rho u}\,\overline{c}_p}\,\frac{L}{D}\right) \tag{24}$$

where $\overline{c}_p$ is the fluid heat capacity, evaluated at the average temperature $\overline{T}$.

Model C: Isothermal Flow. Equation 24 leads to the following two limiting cases depending on the magnitude of the term in the brackets under the exponent. In particular, in the case when $[(4\overline{\alpha})/(\overline{\rho u}\,\overline{c}_p)](L/D)$ is small (practically less than 0.1) the outlet temperature does not depart significantly from the inlet temperature, leading to isothermal flow condition:

$$T_{out} = T_{in} \tag{25}$$

In another limiting case when $[(4\overline{\alpha})/(\overline{\rho u}\,\overline{c}_p)](L/D)$ is significantly large, the outlet temperature approaches the ambient temperature:

$$T_{out} = T_a \tag{26}$$

5. METHODOLOGY

Among the integral models presented in Section 4, model 1A (a combination of models 1 and A) is obtained by integration of eqs 3 to 5 of the rigorous ODSF model presented in Section 3. As such, for relatively short pipeline sections where errors due to averaging of the fluid properties (such as density, heat capacity, and Joule–Thomson coefficient) along the pipeline are relatively small, model 1A can be expected to produce results in closest agreement with the numerical integration of the ODSF model eqs 3 to 5. On the other hand, the pressure drop models 2 and 3 and the thermal models B and C have been proposed for flows of liquids and gases, while ranges of their validity for supercritical CO_2 are not clear. In the present study, in order to clarify this issue, the significance of particular physical effects accounted for by the integral models and the performance of the integral models against the rigorous ODSF model are examined.

Table 1 presents the combinations of the hydraulic and thermal models assessed in the present study. These include nonisothermal models 1A and 1B, compressible isothermal

Table 1. Integral Thermo-Hydraulic Models Examined in the Study

		thermal model		
		A	B	C
	hydraulic model	accounting for heat transfer and expansion cooling (eq 23)	accounting for heat transfer (eq 24)	isothermal flow (eq 25)
1	compressible nonisothermal flow (eq 11)	model 1A	model 1B	–
2	compressible isothermal flow (eq 15)	–	–	model 2C
3	incompressible flow, Darcy–Weisbach equation (eq 17)	model 3A	model 3B	model 3C

DOI: 10.1021/acs.iecr.5b00851
Ind. Eng. Chem. Res. 2015, 54, 8587–8599

model 2C and combinations of Darcy–Weisbach equation (model 3) with the thermal models A, B, and C. As indicated in Table 1, models 1C, 2A, and 2B, which use incompatible assumptions about the temperature variation along the pipeline in the hydraulic and thermal parts of the model, are excluded from the analysis.

The study is performed for conditions of practical relevance to CO_2 pipeline transportation[20] covering inlet pressures, p_{in}, from 90 to 180 bar, the inlet temperatures, T_{in}, from 20 to 60 °C, and the mass flow rates from 1 to 30 Mt/yr.[1] The pipeline internal diameter is varied in the range from 0.4 to 1.2 m, whereas the pipe wall roughness is assumed to be 0.0475 mm. The corresponding pipe wall thickness, d_w, is calculated using the following equation:[9,31]

$$d_w = \frac{P_{MOP} D_o}{2SEF} \tag{27}$$

where P_{MOP}, D_o, S, E, and F are the maximum pipeline operation pressure, the outside pipe diameter, the specified minimum yield stress for the pipe material, the longitudinal joint factor and the design factor, respectively. Following McCoy and Rubin,[9] the parameters in the above equation are set to P_{MOP} = 15.3 MPa, S = 483 MPa, E = 1, and F = 0.72.

In the baseline case, the flow velocity, u_{in}, is set to 3 m/s, which is the average value of the expected range for CO_2 pipeline transportation velocities (1 to 5 m/s).[1] For a pipe of internal diameter D = 0.8 m transporting CO_2 stream with density ρ = 600 kg/m^3, the flow velocity u_{in} = 3 m/s corresponds to the mass flow rate $G = \rho u(1/4)\pi D^2 \sim 30$ Mt/yr. Although this matches with upper bound of the above-mentioned range of transportation flow rates, the effect of smaller flow rates will be investigated for the various pipe diameters in the second part of the Results section. The pipeline length, L, is varied in the range 10 to 100 km, representative of the distances for offshore pipeline transportation in the U.K.

In order to investigate the impact of the pipeline heat exchange with the surrounding, three cases are investigated. These include a perfectly insulated pipeline (adiabatic flow), a buried pipeline, and an uninsulated pipeline exposed to air. When calculating the overall heat transfer coefficient using eq 8, the still air convection heat transfer coefficient, α_a, is set to 5 W/(m^{2}K),[24] whereas in the case of a buried pipeline, the distance between the pipe axis and the ground surface, z_s, is set at 1.4 m. The soil thermal conductivity, λ_s, is assumed to be 1.21 W/(m K).[27] The thermal conductivity of steel material of the pipe wall λ_w is set to 40 W/(m K).

In the next section, firstly, the relative impact of various terms retained in equations of model 1A, on the predicted fluid pressure drop and temperature change, is examined for a representative scenario of transportation of supercritical CO_2 in an uninsulated above-ground pipeline (Section 6.1). This is followed by assessment of accuracy of the integral flow models against predictions by ODSF model of Section 3 for various pipeline flow and heat transfer conditions (Section 6.2).

6. RESULTS AND DISCUSSION

6.1. Analysis of Pressure Drop and Temperature Variation in a Pipe. In order to examine the role of compressibility, viscous friction, heat transfer, and Joule–Thomson effects on the pressure drop and temperature variation in the pipe, the corresponding terms contributing to the integral eqs 11 and 23 of model 1A are evaluated for a flow in uninsulated above-ground pipeline transporting CO_2 at the inlet temperatures T_{in} ranging from 20 to 60 °C. For the sake of an example, it is assumed that the pipeline is 0.8 m in diameter and 20 km long, whereas the inlet velocity is 3 m/s and the inlet pressure is 90 bar.

Figure 2 shows the impact of a change in the inlet temperature on the variations of the pressure drop, $\Delta p = p_{in} - p_{out}$, and its frictional component Δp_{fr} in eq 11 (Figure 2a) as well as the temperature change across the pipe length, $T_{in} - T_{out}$, and its constituencies ΔT_{q_w} and ΔT_{JT} in eq 23 (Figure 2b).

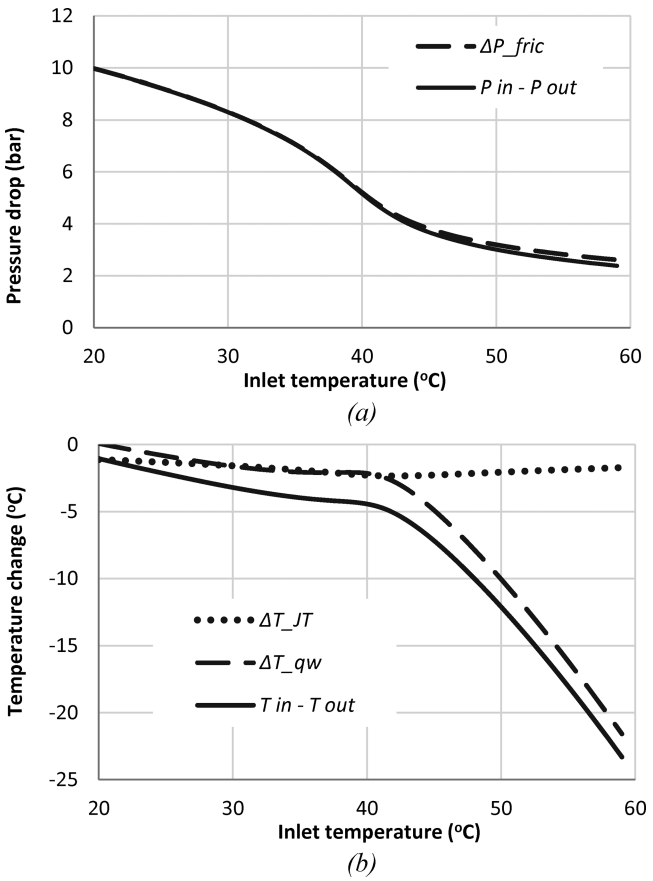

Figure 2. Impact of inlet temperature on (a) the pipeline pressure drop, $p_{in} - p_{out}$, and its frictional component, Δp_{fr} in eq 11, and (b) the temperature change, $T_{in} - T_{out}$, and its components ΔT_{q_w} and ΔT_{JT} in eq 23. Calculations using model 1A for the above-ground pipeline, D = 0.8 m, L = 20 km, p_{in} = 90 bar, u_{in} = 3 m/s.

In particular, Figure 2a shows that the frictional component of the pressure drop, Δp_{fr}, has a major contribution to the overall pressure drop, $\Delta p = p_{in} - p_{out}$. The difference between Δp and Δp_{fr} can be attributed to the compressibility (Δp_c) and density-variation (Δp_ρ) terms in eq 11, which in the present case, makes little contribution to the overall Δp.

Figure 2a also shows that the overall pressure drop gradually decreases with T_{in}. This effect can be attributed to the density decrease with temperature (see Figure 1a), resulting in lower mass flow rates and hence a reduction in the frictional pressure drop, Δp_{fr}.

As can be seen from Figure 2b, ΔT_{JT} is negative (i.e., corresponding to an expansion induced cooling) and is less than 2.5 °C for all the inlet temperatures studied, while the temperature drop associated with the convective cooling

DOI: 10.1021/acs.iecr.5b00851
Ind. Eng. Chem. Res. 2015, 54, 8587–8599

(ΔT_{q_w}) increases with the inlet temperature, and can reach ca. 25 °C at T_{in} = 60 °C. The relatively little variation of ΔT_{JT} with T_{in} is due to opposite effects of T_{in} on the pressure drop and the Joule−Thomson coefficient, μ_{JT}, which both affect ΔT_{JT} in eq 23. In particular, for the studied range of T_{in}, the pipeline pressure drop, Δp, decreases with T_{in} (Figure 2a) while μ_{JT} increases with T_{in} (Figure 1d). As a result, their product, which determine ΔT_{JT} in eq 23 ($\Delta T_{JT} \approx -\mu_{JT}\Delta p$), goes through a local minima and does not change significantly with T_{in}.

In Figure 2b, the nonlinear behavior of ΔT_{q_w} can be explained using a linearized form of eq 24:

$$T_{out} - T_{in} = (T_a - T_{in})\frac{4\alpha}{\overline{\rho u} c_p}\frac{L}{D} \tag{28}$$

which shows that $T_{out} - T_{in}$ is inversely proportional to the fluid heat capacity and is linear with $T_a - T_{in}$. The presence of a local maximum in c_p at T_{in} around 40 °C and 90 bar pressure (see Figure 1, c), is responsible for the nonlinear variation of $T_{out} - T_{in}$ with T_{in} in Figure 2b.

The above observations confirm that for the specific case studied the frictional pressure drop and the heat exchange between the pipe flow and its surrounding have most significant impact on the thermo-hydraulic model predictions. The next section examines the accuracy of the various integral models in more detail for the various conditions relevant to the pipeline transportation.

6.2. Assessment of the Accuracy of the Integral Thermo-Hydraulic Models. To assess the accuracy of the integral thermo-hydraulic models (Table 1), their predictions of the pressure drop, Δp, and the fluid temperature at the outlet of a pipeline, T_{out}, are compared against the corresponding predictions Δp_{ODSF} and $T_{out,ODSF}$ obtained using the rigorous ODSF model based on eqs 3−5.

The relative error of the pressure drop calculations using an integral model is defined as

$$\delta p = 100\%\left(\frac{\Delta p}{\Delta p_{ODSF}} - 1\right) \tag{29}$$

which gives the percentage deviation in the pressure drop from predictions using the rigorous ODSF model. Using the relative error as a measure of accuracy is particularly useful since the scale of pressure drop can be easily estimated (e.g., for horizontal pipes using Darcy−Weisbach eq 17 of model C) to obtain an approximate value of the absolute error of the pressure drop calculations.

Unlike the pressure drop, the temperature variation along the pipe, $T_{in} - T_{out}$, can vary significantly depending on the pipeline heat transfer conditions (as discussed in Section 6.1). For this reason, the relative error of the temperature predictions, defined as

$$\delta T = 100\%\left(\frac{T_{in} - T_{out}}{T_{in} - T_{out,ODSF}} - 1\right) \tag{30}$$

also becomes a strong function of heat transfer conditions. This fact reduces the practical usefulness of the relative error of temperature calculations using the integral models. Hence, it is more convenient to use the absolute difference between the outlet temperatures calculated by an integral and ODSF models as the measure of accuracy:

$$\Delta T = T_{out} - T_{out,ODSF} \tag{31}$$

The rest of this section describes the results of the examination of the impact of flow and heat transfer conditions, as well as the pipe length and diameter on the accuracies of pressure drop and temperature predictions (δp and ΔT) by the various integral thermo-hydraulic models (Table 1).

Effect of Inlet Temperature. Figure 3 shows δp and ΔT calculated using eqs 29 and 31, respectively, based on the simulations using the various models from Table 1 for the inlet temperatures ranging from 20 to 60 °C for a typical 0.8 m internal diameter 20 km long pipeline operating at p_{in} = 90 bar and u_{in} = 3 m/s.

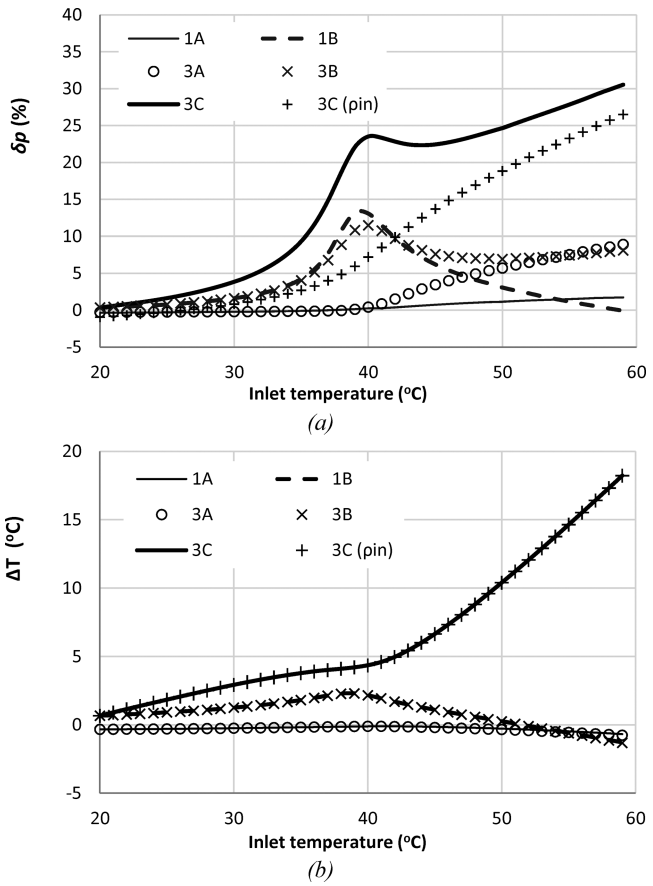

Figure 3. Impact of the inlet temperature on the accuracy of the pipeline pressure drop (a) and outlet temperature (b) predictions by the various thermo-hydraulic models for the above-ground pipeline. D = 0.8 m, L = 20 km, p_{in} = 90 bar, u_{in} = 3 m/s.

Model 1A. The model 1A introduces little inaccuracy in predictions of both the pressure drop (less than 2% in Figure 3a) and the outlet temperature (less than 0.7 °C, Figure 3b). This is expected, as the model 1A retains most terms in the pressure drop and temperature variation equations. As can be seen from Figure 3, model 1A provides the most accurate approximation for the pressure drop and temperature variation in the flow in comparison with predictions using other integral models.

Model 1B. As can be seen from Figure 3b, neglecting the Joule−Thomson effect in model 1B can lead to a slight overestimation of the outlet temperature (ΔT ca. 2.5 °C at T_{in} = 40 °C). In turn, this results in underestimation of the fluid density at the pipe outlet and, hence, overestimation of the

DOI: 10.1021/acs.iecr.5b00851
Ind. Eng. Chem. Res. 2015, 54, 8587−8599

pressure drop (δp up to 13%). The local maxima in δp and ΔT at T_{in} around 40 °C can be attributed to the corresponding local minimum in the variation of ΔT_{JT} with the inlet temperature as discussed in Figure 2b.

Model 3A. The difference between pressure drop predictions by models 3A and 1A (Figure 3a) at T_{in} above ca. 40 °C gradually increases (up to ca. 10% at T_{in} = 60 °C) and can be attributed to the method of calculation of the average density, which in case of eq 11 is obtained as $\overline{p}/\left(\frac{p}{\rho}\right)$, while in eq 17, the density is calculated as a function of $\overline{p}$ and $\overline{T}$.

In Figure 3b, the temperature predictions by model 3A practically coincide with the results obtained by model 1A, which confirms that compressibility of the flow accounted in model 1A has negligible impact on the temperature variation across the pipe length.

Model 3B. In model 3B, similar to model 1B, neglecting the effect of Joule−Thomson cooling results in sight overestimation of the fluid temperature, especially at relatively low operating pressures and high inlet temperatures. In Figure 3a, similar to predictions by model 1B, δp for model 3B reaches its maximum of ca. 12% near T_{in} of 40 °C. At higher inlet temperatures, the pressure drop predictions by model 3A approach the results by model 3A.

The temperature predictions by model 3B coincide with those by model 1B (Figure 3b), as both models use the same eq 24 where the temperature change is a function of the inlet temperature only.

Model 3C. In model 3C the flow is assumed to be isothermal, in which case neglecting the heat transfer term ΔT_{q_w} in eq 23 results in significant overestimation of the outlet temperature, especially for T_{in} above ca. 40 °C (Figure 3b). As discussed with reference to the data in Figure 2, the heat transfer component of the temperature drop can contribute significantly to the overall temperature drop along the pipe. The local maxima in the curve corresponding to model 3C in Figure 3b can be attributed to the neglected Joule−Thomson component of the temperature variation, as discussed above for model 1B.

Overestimation of the fluid temperature in model 3C causes underestimation of the fluid density, leading to significant overestimation (by up to 30%) of pressure drop by eq 17, as can be observed in Figure 3a.

Model 2C. Simulation results obtained based on model 2C were found to be almost identical to those obtained using model 3C. This confirms that for the range of inlet temperatures from 20 to 60 °C and pressures above 90 bar, the pressure drop is dominated by viscous friction, whereas the compressibility term, retained in eq 15, is negligibly small.

Model 3C(ρ_{in}). Because the effect of compressibility has proven to be negligible for the above-studied flow conditions, it is of interest to evaluate the performance of the model 3 where density in eq 17 is taken as constant at the pipeline inlet conditions. Hereafter, the corresponding version of model 3C is referred as model 3C(ρ_{in}).

Because models 3C and 3C(ρ_{in}) use the same heat transfer model, their predictions of the outlet temperature are identical (Figure 3b). In term of the pressure drop predictions (Figure 3a), model 3C(ρ_{in}) gives somewhat more accurate results than model 3C (cf + 7% by model 3C(ρ_{in}) vs +23% by model 3C). The discrepancy between the pressure drop predictions by models 3C and 3C(ρ_{in}) can be related to the fact that fluid pressure drop accounted in the average density predictions by model 3C results in lower values of the fluid density than used by model 3C(ρ_{in}), which in turn is responsible for larger estimates of the pressure drop by eq 17.

The advantage of model 3C(ρ_{in}) is that it uses the inlet density as an estimate of the average density of the fluid in the pipe and hence does not require iterations for the density as a function of the average pressure and temperature defined by eqs 12 and 13. As such, this model is most attractive for use in engineering practice as compared to nonlinear and, hence, more computationally demanding models 1A, 1B, 2C, and 3C. For this reason, the remainder of the paper mostly examines the performance of the model 3C(ρ_{in}).

Effect of Heat Transfer. Figure 4 shows the accuracy of the pressure drop and outlet temperature predictions using model

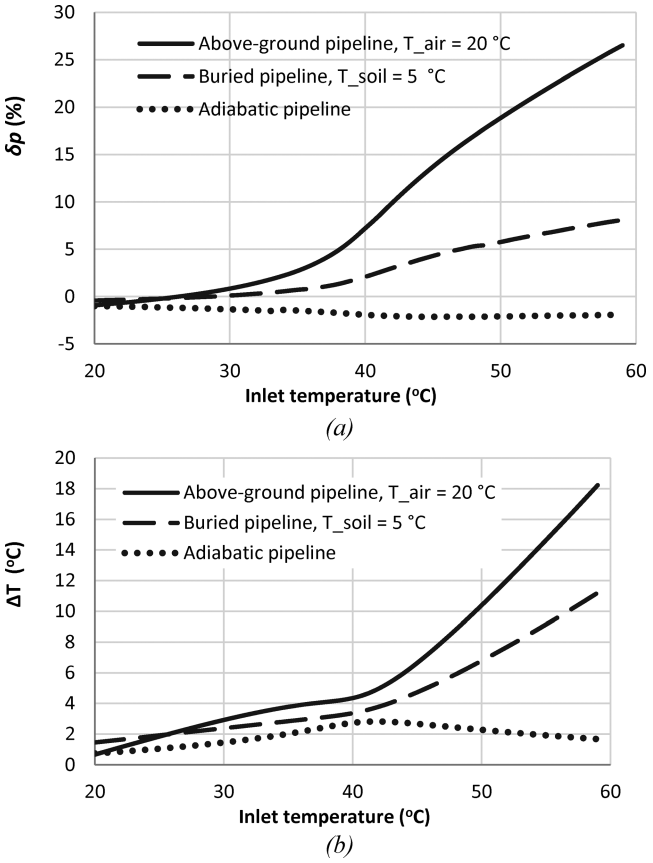

Figure 4. Impact of the inlet temperature and heat transfer conditions on the accuracy of the pipeline pressure drop (a) and outlet temperature (b) predictions by the model 3C(ρ_{in}) [eq 17 is evaluated using density at the pipe inlet]. D = 0.8 m, L = 20 km, p_{in} = 90 bar, u_{in} = 3 m/s.

3C(ρ_{in}) for three different conditions of heat transfer at the pipe wall, corresponding to above-ground uninsulated pipeline, buried noninsulated pipeline and perfectly insulated (adiabatic) pipeline.

In Figure 4b, in the case of flow in insulated (adiabatic) pipeline, the model's inaccuracy of the outlet temperature predictions can be directly attributed to the fact that the model C neglects the Joule−Thomson effect, as discussed in the above for Figure 3. The model 3C(ρ_{in}) also neglects the convective component of temperature variation in the pipe, which explains the observed overestimation of the outlet temperature for

DOI: 10.1021/acs.iecr.5b00851
Ind. Eng. Chem. Res. 2015, 54, 8587−8599

noninsulated, above-ground and buried pipelines, especially at T_{in} above ca. 40 °C (Figure 4b). The outlet temperature overestimation increases with the rate of heat transfer at the pipe wall, which is the largest in the case of the above-ground pipeline and is zero in case of adiabatic pipe.

As discussed in Figure 3, the overestimation of the fluid temperature leads to underestimation of the fluid density and results in overpredictions of pressure drop by eq 17, as can be seen in Figure 4a (by up to 30% in case of above-ground pipeline).

Effect of Inlet Pressure. Figure 5 examines the model 3C(ρ_{in}) when applied for the calculation of flow in the exposed,

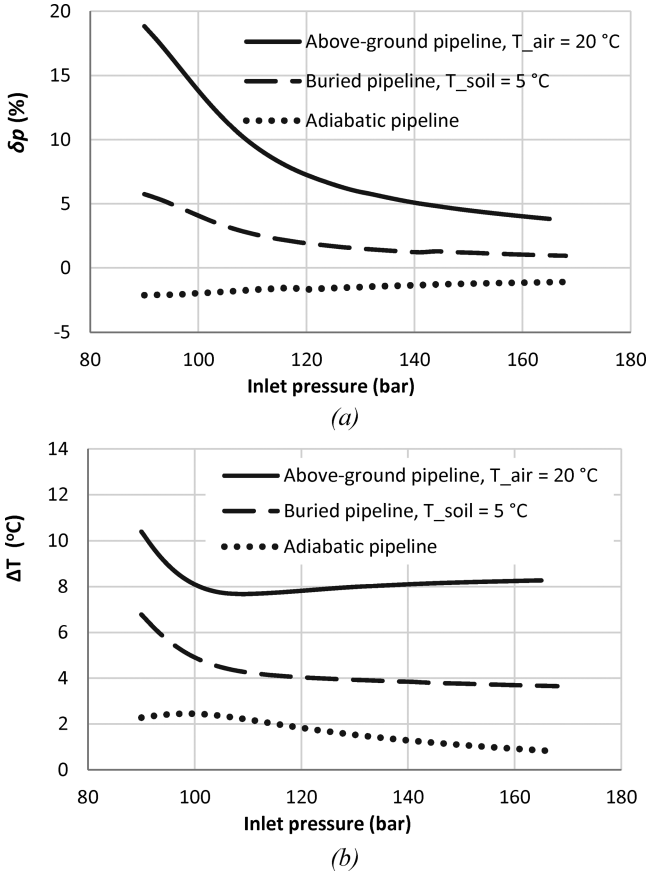

Figure 5. Impact of the inlet pressure and heat transfer conditions on the accuracy of the relative pressure drop (a) and pipeline outlet temperature (b) predictions by the thermo-hydraulic model 3C(ρ_{in}) [eq 17 is evaluated using density at the pipe inlet]. L = 20 km, T_{in} = 50 °C, u_{in} = 3 m/s.

buried and adiabatic pipelines with the inlet temperature, T_{in}, of 50 °C and the inlet pressures, p_{in}, ranging from 90 to 170 bar. As it may be observed from the data, the accuracy of the pressure drop predictions (Figure 5a) improves with the increase in the inlet pressure, most significantly for the case of above-ground pipeline (δp decreases from ca. 18% to 4% when p_{in} increases from 90 to 170 bar). On the other hand, Figure 5b shows that inlet pressure has nonmonotonous and relatively small impact on the predicted outlet temperature for all the three heat transfer cases examined.

Effect of Pipe Length. Figure 6 shows impact of pipe length on the accuracy of the pressure drop and outlet temperature predictions using two variations of model 3C, namely, model 3C(ρ_{in}) and model 3C with the density evaluated at ambient

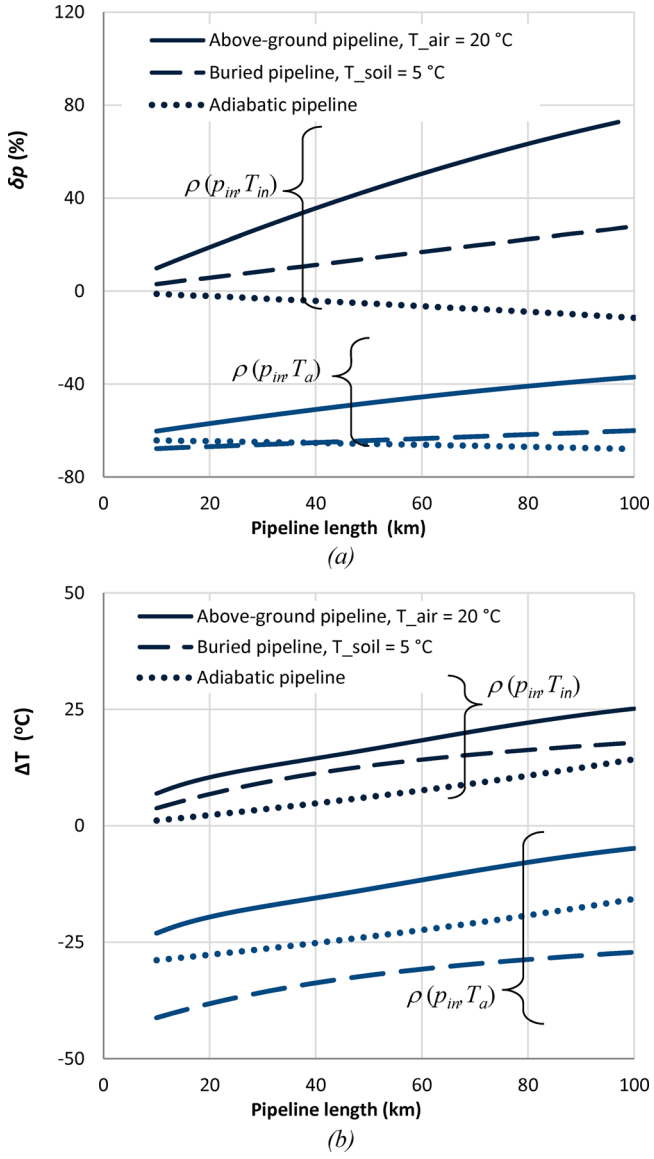

Figure 6. Impact of the pipe length and heat transfer conditions on the accuracy of the relative pressure drop (a) and pipeline outlet temperature (b) predictions by the thermo-hydraulic model 3C(ρ_{in}) and model 3C with the density evaluated at ambient temperature $\overline{\rho}$ = $\rho(p_{in}, T_a)$. T_a = 20 °C for the above-ground pipe and T_a = 5 °C for the buried pipe. T_{in} = 50 °C, p_{in} = 90 bar, G = 13.7 (Mt/yr).

temperature $\overline{\rho}$ = $\rho(p_{in}, T_a)$. The results were obtained for the above-ground, buried and adiabatic pipelines.

As it may be observed in Figure 6, when using model 3C(ρ_{in}), as the pipeline length increases, the accuracy of both the pressure drop and temperature predictions deteriorates. In particular, Figure 6b shows that ΔT increases with the pipeline length. This trend can be attributed to smaller outlet temperatures, $T_{out,ODSF}$, predicted by ODSF model for longer pipelines. In turn, the increase in ΔT results in larger underestimates of the fluid density in eq 17, leading to larger errors in the pressure drop estimate (Figure 6a). In agreement with the observation made for Figure 4, model 3C(ρ_{in}) has the lowest accuracy both in terms of the pressure drop and temperature predictions in the case of the above-ground pipe. Here, as the pipeline length increases from 10 to 100 km, the

DOI: 10.1021/acs.iecr.5b00851
Ind. Eng. Chem. Res. 2015, 54, 8587−8599

values of δp and ΔT increase from 10 to 80% and from 6 to 25 °C respectively.

Figure 6 also shows that in contrast with the trend observed for model 3C(ρ_{in}), the accuracy of model 3C with the density defined at ambient temperature T_a, improves as the pipeline length increases. For the above-ground pipelines longer than ca. 60 km, model 3C with the density defined at ambient temperature T_a, provides results that are more accurate than model 3C(ρ_{in}) .

The above trends can be explained by examining eq 24, which turns into eqs 25 and 26 depending on the order of magnitude of the characteristic length scale $(\overline{\rho u}\,\overline{c}_p D)/(4\overline{\alpha})$. The latter can be estimated to be in the range from ca. 20 km for warm CO_2 streams at 90 bar inlet pressure to ca. 400 km for cooler dense-phase streams. As such, for relatively short pipes (L = 20−50 km) and high pressures the ratio $(4\overline{\alpha})/(\overline{\rho u}\,\overline{c}_p)(L/D)$ can be expected to be relatively small, justifying the use of eq 25 ($T_{out} = T_{in}$). In case of pipelines transporting relatively warm streams at pressures below 90 bar, the ratio $(4\overline{\alpha})/(\overline{\rho u}\,\overline{c}_p)(L/D)$ may increase, so that eq 25 will lose its validity. Only for very long pipelines, extending in lengths beyond 150 km, the ratio $(4\overline{\alpha})/(\overline{\rho u}\,\overline{c}_p)(L/D)$ can become large enough so that approximation $T_{out} = T_a$ becomes valid.

Effect of Pipe Diameter and Flow Rate. Figures 7a,b show, respectively, the accuracy of the pressure drop and temperature predictions using model 3C(ρ_{in}) for various pipeline diameters and range of flow rates from 1 to 30 Mt/yr, which are relevant to CCS.[1] For example, the results are obtained assuming a 20 km long buried pipeline, transporting CO_2 at inlet pressure of 90 bar and inlet temperature of 50 °C. For these inlet conditions and the pipe diameters ranging from 0.4 to 1.2 m, the corresponding inlet velocities vary in the range from 0 to ca. 1 m/s.

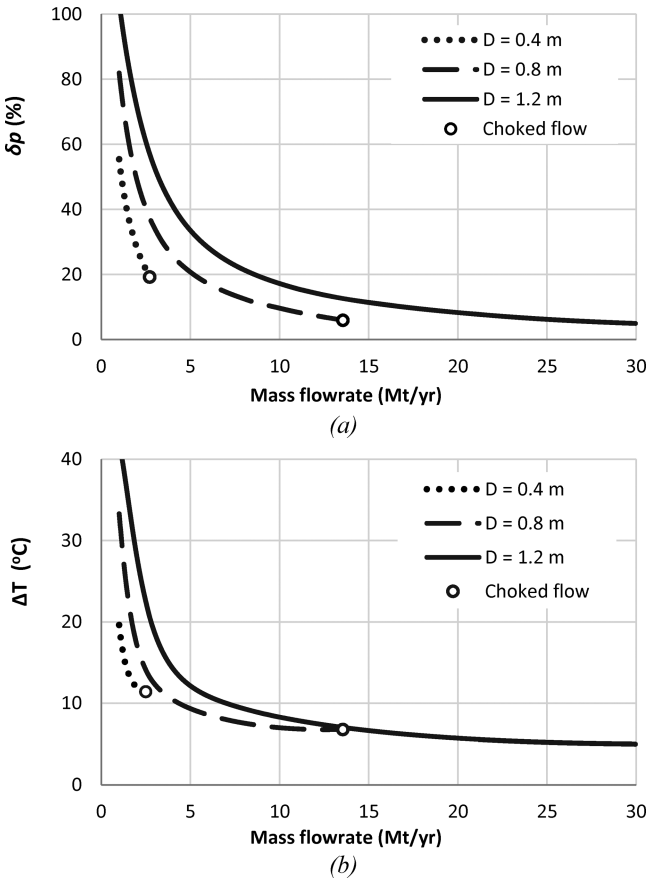

Figure 7. Impact of the mass flow rate and pipeline diameter on the accuracy of the pipeline pressure drop (a) and outlet temperature (b) predictions by the thermo-hydraulic model 3C(ρ_{in}) with the density in eq 17 calculated at the pipe inlet pressure and temperature. Buried pipeline, T_{soil} = 5 °C, L = 20 km, p_{in}= 90 bar, T_{in} = 50 °C.

Figure 7 shows that as the flow rate increases and the pipeline diameter decreases, the errors in the pressure and temperature predictions by model 3C(ρ_{in}) become smaller. It can be noted that the trends observed in Figure 7a are similar to those in Figure 7b. As discussed earlier in Figure 3, this is due to the fact that errors in the fluid temperature predictions directly affects the accuracy of the pressure drop calculation by Model 3C. The variation of the ΔT with the mass flow rate and the pipe diameter in Figure 7b can be explained using eq 24, which shows that increasing the flow rate ($G = \rho u(1/4)\pi D^2$) reduces the temperature gradient in a pipe, making the flow closer to isothermal at the inlet temperature, as assumed in model 3C(ρ_{in}).

In practical terms, Figure 7 shows that model 3C(ρ_{in}) gives better accuracy at higher flow rates and smaller pipeline diameters. At flow rates less than 5 Mt/yr, the model can overestimate the pressure drop by more than 30% and temperature by more than 10 °C.

Figure 7 also shows that increasing the flow rate in pipelines of diameter D = 0.4 and 0.8 m may lead to choked flow, as predicted by ODSF model and marked by circles on the curves. Because the choked flow conditions cannot be simulated using any of the above integral models, extra care should be taken when using them for long pipes of small diameters and large mass flow rates.

7. CONCLUSIONS AND DISCUSSION

This work was aimed to assess the accuracy of a number of commonly used integral thermo-hydraulic models for the calculations of pressure and temperature variations in pipelines transporting dense-phase and supercritical CO_2. The integral models of different complexity, accounting for various physical effects (compressibility, expansion cooling, and heat transfer), were examined by comparing the simulation results with predictions using a more rigorous ODSF model.

The analysis of predictions by ODSF model of a flow in a 0.8 m diameter and 20 km long pipe showed that in case when CO_2 enters the pipeline in a supercritical state at temperatures of 40−60 °C (conditions practically relevant to CCS[23−25,27]), the expansion cooling of the fluid and heat transfer at the wall can be significant, contributing in total by as much as 20 °C to the temperature change in the flow. Neglecting such variations in the fluid temperature is shown to result in under-prediction of the fluid density and significant overestimations (up to ca. 30%) of the pipeline pressure drop. In practice, this can lead to substantial overdesign of the pipeline, which may involve using thicker-wall pipes and larger number of compressor/pump stations along the pipeline route than necessary. For example, for a flow of CO_2 in a realistic pipeline with an average pressure gradient of 0.5 bar/km and length of 200 km, the 30% inaccuracy in the pressure drop estimate translates into 30 bar extra pressure loss in the pipeline. Compensating this extra pressure drop would require the installation of a booster pump station, adding extra costs to the pipeline construction and operation. To avoid losing accuracy in the outlet temperature

DOI: 10.1021/acs.iecr.5b00851
Ind. Eng. Chem. Res. 2015, 54, 8587−8599

estimates, the effects of thermal expansion and, most importantly, the heat transfer to the flow at the pipe wall should be both taken into account in the temperature equation of thermo-hydraulic model.

The analysis of the integral flow models showed that model 1A based on the nonisothermal compressible flow equation for the pressure drop, combined with the temperature equation accounting for the Joule−Thomson effect and heat exchange at the pipe wall, can be recommended for accurate predictions of pipeline pressure drop and temperature variation in relatively short pipes as alternative to ODSF model. Because the model 1A equations are nonlinear, they can only be solved numerically. This model is valid for a wide range of temperatures and pressures relevant to transport of supercritical and dense-phase CO_2. In the case of supercritical fluid, a simple criterion $L < L_{ch}$ based on eq 14 can be applied to ensure that the flow remains subsonic in the pipe.

Model 1B uses the same nonlinear pressure drop equation as model 1A but a simpler temperature equation which neglects the Joule−Thomson effect. The latter assumption results only in a slight loss in accuracy of the temperature and pressure drop predictions by the model; however, from the computational point of view, there is no advantage in using model 1B in comparison with model 1A.

Models 3A and 3B are based on the Darcy−Weisbach equation for the frictional pressure drop, which is much simpler to solve compared with the nonlinear integral momentum equation in model 1A. Both models 3A and 3B capture the temperature variation in the flow due to the heat exchange between the pipeline and its surrounding, which is important to get accurate estimate of the average fluid density and the pressure drop across the pipeline. Accounting for the Joule−Thomson effect in model 3A allows slightly more accurate fluid temperature predictions compared with model 3B. These models are recommended for prediction of a pressure drop in dense-phase and supercritical CO_2 in relatively short pipelines where the flow can be treated as incompressible along the entire length of the pipe. While the latter would almost always apply to low-velocity transport of dense-phase CO_2, in the case of supercritical fluid the incompressibility assumption puts a strong constraint on the pipeline length, which should remain well below the "critical" length, L_{ch}, that can be estimated using eq 14.

Model 3C is the simplest of the integral models examined. It assumes an isothermal flow in a pipe and uses the Darcy−Weisbach equation for the frictional pressure drop. In the case of low-velocity flows in relatively short pipeline sections (20−40km), the fluid behaves as incompressible, and hence, the Model 3C predictions match very well with predictions using the more rigorous Model 2C accounting for compressibility effect. Three variations of model 3C are due to three different methods for calculation of the average density in the Darcy−Weisbach equation. The basic method uses the density evaluated at the mean average pressure and inlet temperature, and hence requires iterations to solve nonlinear equation for the pipeline outlet pressure. This model predicts the pressure drop within 8% agreement with the predictions by the ODSF model for CO_2 streams at inlet temperatures in the range 20−60 °C and pressures above 90 bar. The model accuracy improves with the decrease in the pipe length and increase in fluid inlet pressure. In model 3C(ρ_{in}) the average density in Darcy−Weisbach equation is taken at the pipe inlet pressure and temperature, and hence the model provides noniterative solution for the pressure drop. This approximation is particularly useful for relatively short pipelines (10−20 km) transporting dense-phase CO_2. In the third version of model 3C, the density is evaluated at the pipe inlet pressure and ambient temperature. This method gives more accurate estimates of pressure drop in long pipelines, extending above ca. 100 km.

In conclusion, the integral thermo-hydraulic model based on the Darcy−Weisbach equation combined with the equation for the fluid temperature variation along the pipe accounting for effects of thermal expansion and heat transfer, can be recommended for conservative, though rather accurate, estimates of pressure drop in design calculations of horizontal CO_2 transportation pipelines.

It should be noted that the integral flow models considered in the present study have certain limitations. In particular, although they can account for compressible nature of the fluid, they do not resolve the flow profiles along the pipe, and hence, they cannot be used to predict reliably the choked flow. As such, care should be taken when using integral model for long pipes of small diameters and large mass flowrates. Also, the study examines the integral models describing steady-state single-phase CO_2 flows at pressures above the critical pressure of CO_2. In the case of CO_2 transportation at lower pressures, the choice of the integral models is more conventional; that is, compressible nonisothermal flow model (model 1A) can be recommended for gas-phase flows, while incompressible isothermal flow (model 3C) would be the natural choice for liquid-phase flows. In all the cases, the results of predictions using the above models should be checked to ensure the flow remains single-phase along the entire length of the pipeline.

AUTHOR INFORMATION

Corresponding Authors

*E-mail: s.martynov@ucl.ac.uk.
*E-mail: h.mahgerefteh@ucl.ac.uk.

Notes

The authors declare no competing financial interest.

ACKNOWLEDGMENTS

The research leading to this work has received funding from the European Union Seventh Framework Programme FP7-ENERGY-2012-1-2STAGE under grant agreement number 309102.

NOMENCLATURE

c_p = specific heat capacity (J kg^{-1} K^{-1})
c_s = adiabatic speed of sound (m s^{-1})
d_w = the pipe wall thickness (m)
D = pipeline internal diameter (m)
D_o = pipeline external diameter (m)
E = the longitudinal joint factor in eq 27
f = the Darcy friction factor
F = design factor in eq 27
$G = \rho u(1/4)\pi D^2$ = mass flow rate (kg s^{-1})
h = specific enthalpy (J kg^{-1})
L = pipeline length (m)
M = the Mach number
p = pressure (Pa)
$Pr_f = \mu c_p / \lambda_f$ = the Prandtl number
P_{MOP} = the maximum pipeline operation pressure (Pa)
q_w = the heat flux at the pipe wall (W m^{-2})

DOI: 10.1021/acs.iecr.5b00851
Ind. Eng. Chem. Res. 2015, 54, 8587−8599

R = the gas constant of CO_2 (J mol^{-1} K^{-1})
Re = $\overline{\rho u}D/\mu_f$ = the Reynolds number
S = the specified minimum yield stress for the pipe material (Pa)
T = temperature (°C)
u = flow velocity (m s^{-1})
x = coordinate along the pipeline (m)
Z = compressibility factor
z_s = the depth at which the pipeline is buried (m)
$\Delta p = p_{in} - p_{out}$ = overall pressure drop along the pipe (Pa)
Δp_ϑ, $\Delta p_\mathcal{O}$, Δp_ρ = components of pressure drop in eq 10 (Pa)
ΔT_{q_w} and ΔT_{JT} = constituencies of $(T_{in} - T_{out})$ in eq 23 (°C)
$\Delta T = T_{out} - T_{out,ODSF}$ = absolute error of temperature predictions, eq 31 (°C)

Greek Symbols

α = overall heat transfer coefficient (W m^{-2} s^{-1})
ϵ = wall roughness (m)
γ = adiabatic index
λ = thermal conductivity (W m^{-1} K^{-1})
μ_{JT} = the Joule-Thomson coefficient (°C Pa^{-1})
μ_f = coefficient of the dynamic viscosity (Pa m^{-1})
$\overline{\rho u}$ = average mass flux (kg m^{-2} s^{-1})
ρ = density (kg m^{-3})
δp = relative error of the pressure drop calculations, defined by eq 29
δT = relative error of the temperature calculations, defined by eq 30

Indexes

a = the media surrounding the pipe
f = the fluid inside the pipe
fr = frictional pressure drop
in = at the pipe inlet
out = at the pipe outlet
s = the soil
w = the pipe wall
ODSF = based on the ODSF model

Abbreviations

CCS = Carbon Capture and Sequestration
ODSF = one-dimensional steady-state flow
1A - 3C = thermo-hydraulic models listed in Table 1

REFERENCES

(1) *IPCC Special Report on Carbon Dioxide Capture and Storage. Prepared by Working Group III of the Intergovernmental Panel on Climate Change*; Metz, B.; Davidson, O.; de Concick, H. C.; Loos, M.; Middleton, R. S., Eds.; Cambridge University Press: Cambridge, 2005.
(2) MacDowell, N.; Florin, N.; Buchard, A.; Hallett, J.; Galindo, A.; Jackson, G.; Adjiman, C. S.; Williams, C. K.; Shah, N.; Fennell, P. An overview of CO_2 capture technologies. *Energy Environ. Sci.* **2010**, *3* (11), 1645−1669.
(3) Boot-Handford, M. E.; Abanades, J. C.; Anthony, E. J.; Blunt, M. J.; Brandani, S.; Mac Dowell, N.; Fernandez, J. R.; Ferrari, M. C.; Gross, R.; Hallett, J. P.; et al. Carbon capture and storage update. *Energy Environ. Sci.* **2014**, *7* (1), 130−189.
(4) White Rose Carbon Capture & Storage Project. http://www.whiteroseccs.co.uk/ (accessed January 16, 2015).
(5) Peterhead CCS project. http://www.shell.co.uk/gbr/environment-society/environment-tpkg/peterhead-ccs-project.html (accessed January 16, 2015).
(6) Boundary Dam Carbon Capture Project. http://www.saskpowerccs.com/ccs-projects/boundary-dam-carbon-capture-project/ (accessed June 4, 2015).
(7) Petra Nova: W.A. Parish Post-Combustion CO_2 Capture and Sequestration Project. http://www.netl.doe.gov/research/coal/major-demonstrations/clean-coal-power-initiative/ccpi-petra-nova?k=FE0003311 (accessed June 4, 2015).
(8) Recht, D. L. Design considerations for carbon-dioxide pipe lines. 1. Pipe Line Industry. *Pipeline Gas Journal* **1984**, *61* (3), 53−54.
(9) McCoy, S. T.; Rubin, E. S. An engineering-economic model of pipeline transport of CO_2 with application to carbon capture and storage. *Int. J. Greenhouse Gas Control* **2008**, *2* (2), 219−229.
(10) Rubin, E. S.; Chen, C.; Rao, A. B. Cost and performance of fossil fuel power plants with CO_2 capture and storage. *Energy Policy* **2007**, *35* (9), 4444−4454.
(11) Parfomak, P. W.; Folger, P. *Carbon Dioxide (CO_2) Pipelines for Carbon Sequestration: Emerging Policy Issues*. CRC Report for Congress RL33971. Congressional Research Service, Library of Congress: Washington, DC, 2007.
(12) Davison, J. Performance and costs of power plants with capture and storage of CO_2. *Energy* **2007**, *32* (7), 1163−1176.
(13) *Energy Technology Perspectives. Harnessing Electricity's Potential*. OECD/IEA: 2014. http://www.iea.org/bookshop/472-Energy_Technology_Perspectives_2014 (accessed June 4, 2014).
(14) *Climate Change 2014: Mitigation of Climate Change. Contribution of Working Group III contribution to the 5th Assessment Report of the Intergovernmental Panel on Climate Change*; Cambridge University Press: Cambridge, 2013.
(15) *The Potential for Reducing the Costs of CCS in the UK. CCS Cost Reduction Task Force Final Report*. Department of Energy & Climate Change: London, 2013.
(16) Skovholt, O. CO_2 transportation system. *Energy Convers. Manage.* **1993**, *34* (9−11), 1095−1103.
(17) *Building the cost curves for CO_2 storage: European sector*; International Energy Agency Greenhouse Gas R&D Programme: February 17, 2005.
(18) Vandeginste, V.; Piessens, K. Pipeline design for a least-cost router application for CO_2 transport in the CO_2 sequestration cycle. *Int. J. Greenhouse Gas Control* **2008**, *2* (4), 571−581.
(19) Serpa, J.; Morbee, J.; Tzimas, E. *Technical and Economic Characteristics of a CO_2 Transmission Pipeline Infrastructure*; European Commission, Joint Research Centre, Institute for Energy. Publications Office of the European Union: Luxembourg, 2011.
(20) Chandel, M. K.; Pratson, L. F.; Williams, E. Potential economies of scale in CO_2 transport through use of a trunk pipeline. *Energy Convers. Manage.* **2010**, *51* (12), 2825−2834.
(21) Knoope, M. M. J.; Ramirez, A.; Faaij, A. P. C. Economic Optimization of CO_2 Pipeline Configurations. *Energy Procedia* **2013**, *37* (0), 3105−3112.
(22) Wang, Z.; Cardenas, G. I.; Fimbres Weihs, G. A.; Wiley, D. E. Optimal Pipeline Design with Increasing CO_2 Flow Rates. *Energy Procedia* **2013**, *37* (0), 3089−3096.
(23) Liljemark, S.; Arvidsson, K.; Mc Cann, M. T. P.; Tummescheit, H.; Velut, S. Dynamic simulation of a carbon dioxide transfer pipeline for analysis of normal operation and failure modes. *Energy Procedia* **2011**, *4* (0), 3040−3047.
(24) Zhang, Z. X.; Wang, G. X.; Massarotto, P.; Rudolph, V. Optimization of pipeline transport for CO2 sequestration. *Energy Convers. Manage.* **2006**, *47* (6), 702−715.
(25) Seevam, P. N.; Race, J. M.; Downie, M. J.; Hopkins, P. *Transporting the next generation of CO2 for carbon, capture and storage: the impact of impurities on supercritical CO_2 pipelines*; ASME Press: New York, 2008; pp 39−51.
(26) Chaczykowski, M.; Osiadacz, A. J. Comparative assesment of steady-state pipeline gas flow models. *Arch. Min. Sci.* **2012**, *57* (1), 23−38.
(27) Witkowski, A.; Rusin, A.; Majkut, M.; Rulik, S.; Stolecka, K. Comprehensive analysis of pipeline transportation systems for CO_2 sequestration. Thermodynamics and safety problems. *Energy Convers. Manage.* **2013**, *76* (0), 665−673.
(28) de Medeiros, J. L.; Versiani, B. M.; Araujo, Q. F. A model for pipeline transportation of supercritical CO2 for geological storage. *Journal of Pipeline Engineering* **2008**, 253.

DOI: 10.1021/acs.iecr.5b00851
Ind. Eng. Chem. Res. 2015, 54, 8587−8599

(29) Dongjie, Z.; Zhe, W.; Jining, S.; Lili, Z.; Zheng, L. Economic evaluation of CO_2 pipeline transport in China. *Energy Convers. Manage.* **2012**, *55* (0), 127−135.
(30) Bagajewicz, M.; Valtinson, G. Computation of Natural Gas Pipeline Hydraulics. *Ind. Eng. Chem. Res.* **2014**, *53* (26), 10707−10720.
(31) Menon, E. S. *Gas Pipeline Hydraulics*; CRC Press: Boca Raton, FL, 2005.
(32) Branan, C. R. *Rules of Thumb for Chemical Engineers. Section One. Equipment Design. 1. Fluid Flow*, 5th ed.; Butterworth-Heinemann: Oxford, UK, 2012.
(33) Ghazi, N.; Race, J. M. Techno-economic modelling and analysis of CO_2 pipelines. *Proceedings of the 9th International Pipeline Conference*. Calgary, Alberta, Canada, September 24−28, 2012; Paper No. IPC2012−90455.
(34) *Development of a global CO_2 pipeline infrastructure*; International Energy Agency Greenhouse Gas R&D Programme: 01 August 2010.
(35) Mohitpour, M.; Golshan, H.; Murray, M. A. *Pipeline Design & Construction: A Practical Approach*; ASME Press: New York, 2007.
(36) Nimtz, M.; Klatt, M.; Wiese, B.; Kuhn, M.; Joachim Krautz, H. Modelling of the CO2 process- and transport chain in CCS systems. Examination of transport and storage processes. *Chem. Erde* **2010**, *70* (Supplement3), 185−192.
(37) *NIST Standard Reference Database 23. NIST Reference Fluid Thermodynamic and Transport Properties Database (REFPROP)*, version 9.1; http://www.nist.gov/srd/nist23.cfm (accessed June 4, 2015).
(38) Wei, Y. S.; Sadus, R. J. Equations of state for the calculation of fluid-phase equilibria. *AIChE J.* **2000**, *46* (1), 169−196.
(39) Li, H.; Yan, J. Evaluating cubic equations of state for calculation of vapor-liquid equilibrium of CO_2 and CO_2-mixtures for CO_2 capture and storage processes. *Appl. Energy* **2009**, *86* (6), 826−836.
(40) Span, R.; Wagner, W. A new equation of state for carbon dioxide covering the fluid region from the triple-point temperature to 1100 K at pressures up to 800 MPa. *J. Phys. Chem. Ref. Data* **1996**, *25* (6), 1509−1596.
(41) Lurie, M. V. *Modeling of Oil Product and Gas Pipeline Transportation*; Wiley-VCH Verlag GmbH & Co. KGaA: Weinheim, 2008.
(42) Coulson, J. M.; Richardson, J. F.; Backhurst, J. R.; Harker, J. H. *Chemical Engineering*, 6th ed.; Elsevier: Oxford, 1999.
(43) Incropera, F. P.; DeWitt, D. P. *Introduction to Heat Transfer*; 3rd ed.; John Wiley & Sons, Inc.: New York, 1996.
(44) Petzold, L. *Differential Algebraic System Solver*. DASSL. 1991; http://www.engineering.ucsb.edu/~cse/software.html (accessed January 4, 2015).
(45) Hamelinck, C. N.; Faaij, A. P. C.; Turkenburg, W. C.; van Bergen, F.; Pagnier, H. J. M.; Barzandji, O. H. M.; Wolf, K. H. A. A.; Ruijg, G. J. CO_2 enhanced coalbed methane production in the Netherlands. *Energy* **2002**, *27* (7), 647−674.
(46) Heddle, G.; Herzog, H.; Klett, M. *The Economics of CO_2 Storage*; Report LFEE 2003−003 RP; Massachusetts Institute of Technology, Laboratory for Energy and the Environment: Cambridge, MA, Aug, 2003.
(47) *Pipeline transmission of CO_2 and energy*. Report Number PH 4/6.; International Energy Agency Greenhouse Gas R&D Programme: 2002.
(48) Kurganov, V. A. Pressure drop, Single-phase. *THERMOPEDIA(TM) A-to-Z. Guide to Thermodynamics, Heat & Mass Transfer, and Fluids Engineering* [Online]; Posted Feb 2, 2011. http://www.thermopedia.com/content/1055/ (accessed March 16, **2014**).
(49) Anderson, J. D. *Modern Comprssible Flow: With Historical Perspective*, 3rd ed.; McGraw-Hill: London, 2004.

DOI: 10.1021/acs.iecr.5b00851
Ind. Eng. Chem. Res. 2015, 54, 8587−8599